Contents lists available at ScienceDirect

Computers and Electronics in Agriculture
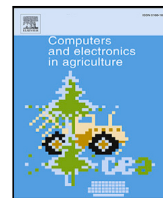
Original papers

Standing tree health assessment using contact–ultrasonic testing and machine learning

Mohsen Mousavi [a], Mohammad Sadegh Taskhiri [b], Amir H. Gandomi [a,c,*]

[a] *Faculty of Engineering and IT, University of Technology Sydney, Ultimo, NSW 2007, Australia*
[b] *Commonwealth Scientific and Industrial Research Organisation (CSIRO), Canberra, Australia*
[c] *University Research and Innovation Center (EKIK), Óbuda University, 1034 Budapest, Hungary*

ARTICLE INFO

ABSTRACT

The problem of hole-defect detection in standing trees is solved. An ultrasonic device (Pundit PL-200) was employed to collect ultrasonic signals from various wood specimens both in the lab and field. The collected ultrasonic signals were then processed through the Variational Mode Decomposition algorithm to derive effective features. In order to solve the classification problem more efficiently, the obtained characteristics were then analyzed through PCA to determine the most useful features. Several machine learning algorithms and a one-dimensional convolutional neural network (1D-CNN) were employed to solve a set of classification problems based on data collected from (1) specimens with artificial defects in the lab and (2) billets with natural defects selected from trees harvested at sites in the two states of WA and NSW, Australia. The results demonstrate the effectiveness of the proposed method for classifying wood materials based on their health state, where testing accuracy results of 100% in the lab and at least 92.2% in fields were achieved. The Fine Gaussian SVM was found to perform most effectively on data derived from specimens in the lab and fields. It was also shown that 1D-CNN results were more reliable for generalizing the solution to the classification problem of standing trees in fields.

1. Introduction

Modern detection and diagnosis (FDD) systems involve several steps, including (1) system knowledge representation, (2) data acquisition and signal processing, (3) fault classification, and (4) maintenance-related decision-making (Abid et al., 2021). Traditionally, the decay assessment of trees involves visual inspection to identify external evidence of structural failure. Such signs include wounds on self-pruned branches, which can occur if trees are not pruned in time and subsequently undergo a self-pruning process. Some invasive methods are used for decay detection in standing trees, such as decay detection drill (Goh et al., 2018). As such, a noninvasive sensing technology for detecting wood defects in standing trees is yet to be developed.

Monitoring wood quality is of paramount interest to the mechanized harvesting industry (Palander et al., 2018). For instance, it is known that knot clusters can affect the mechanical properties of wood products (Pang et al., 2021). Wood material assessment favors the extensive development of novel nondestructive techniques developed over the past decades. Such techniques usually comprise two elements: a sensing technology for collecting data of a wooden specimen and a data analysis algorithm that can interpret such data by deriving some

features that can characterize the health state of the wood. Some of such sensing technologies include ultrasonics (Yang and Yu, 2017), thermography (López et al., 2013), and radiography (Li et al., 2014). Ultrasonic testing has been widely used for quality assessment of wood materials (Blomme et al., 2002) due to the following reasons: (1) it is a less invasive and less expensive technique compared to other methods, and (2) it is susceptible to the existence of defects in wood materials (Senalik et al., 2014). Therefore, they have been used in several research for quality assessment of wooden sections (Tallavo et al., 2012; Gao et al., 2014; Fang et al., 2017). For instance, the capability of ultrasonic techniques for evaluating mechanical properties of wood with artificial defects has been demonstrated in several studies (Reinprecht and Pánek, 2012; Mori et al., 2016). Ultrasonic tomography was also demonstrated as an effective method for detecting defects in standing trees (Lin et al., 2008), where it was shown that the velocity of the ultrasonic waves was correlated with the ratio of the hole-to-disc area. Another study found that the attenuation of the ultrasonic wave velocity and increased damping could be correlated with the presence of a defect in standing trees (Krajnc et al., 2019). However, it was also learned that both ultrasound velocity and damping were sensitive to the

---

diameter at the breast height (DBH) of the studied tree. A binary logistic regression was developed to explore the possibility of using ultrasound velocity and damping to predict internal defects' presence in stating trees (Krajnc et al., 2019). The obtained accuracy using the velocity and damping were respectively 0.72 and 0.76 in European beech and 0.83 and 0.82 in Norway spruce spices. Studying the time of flight of the ultrasonic waves traveling across the wood sections has also been demonstrated effective for evaluating defects in standing trees.

Generally, there are two ways to study wood using ultrasonic techniques. The first approach that considers a close study of the underlying physics is guided wave technology (GWT). It allows inspection of an elongated member by guiding ultrasound through the member's boundaries. The proper probing frequency varies from 20 to 100 kHz depending on the study member's size and thickness (Pedram et al., 2018). Further, this method uses dispersion curves as graphic representations of advanced mathematical modeling. Fathi et al. (2021) showed that semi-analytically derived dispersion curves were in excellent agreement with measured Lamb wave velocities for wood specimens of different moisture content (MC). The propagation of lamb waves and mechanical three-point bending tests were conducted on green poplar wood specimens with varying MC. Lamb wave modes were propagated in specimens using ultrasonic actuators, and wave signals were acquired using an ultrasonic sensor along the propagation direction of the specimens. The measured Lamb wave velocity was consistent with semi-analytically calculated dispersion curves (less than 2% difference) for wood specimens with various MCs.

Nonetheless, guided waves are complex, and solving the wave equation for structures made of orthotopic materials, such as wooden poles, is still challenging (Dackermann et al., 2014). As a result, GWUT cannot be relied upon to interpret the wave patterns extracted from these structures based on field measurements. In recent years, GWUT test results have been interpreted using machine learning-based methods to resolve its shortcomings. For example, Fathi et al. (2020) applied the guided Lamb wave propagation method to predict the modulus of elasticity and modulus of rupture of wood with varying moisture content (MC) by developing a machine-learning model. They combined the "group method of data handling" with Lamb wave velocity to predict wood's mechanical properties, namely the modulus of rupture (MOR) and modulus of elasticity (MOE). The results of analyzing 70 green poplar wood specimens demonstrate that wood's MC, density, and mechanical properties are highly correlated with Lamb wave velocity. As a result, guided Lamb wave propagation can be used for the nondestructive characterization of timber. Nasir et al. (2021) also implemented machine learning algorithms to determine the MOR and MOE in UV-degraded wood sections using decision trees.

Conventional ultrasonic techniques diagnose material properties by measuring the velocity and time of flight of bulk waves propagating within them (Yaitskova and van de Kuilen, 2014; Karaiskos et al., 2015). Time-domain characteristics of other forms of NDT techniques, such as Hz Time-Domain sensing (Lei et al., 2022), have also been used for wood quality assessment. However, wood's orthotropic nature depends on the testing direction (Mackenzie-Helnwein et al., 2003; Liu et al., 2013), which results in independent mechanical properties on three perpendicular axes. These axes include (1) longitudinally along the fibers/grain, (2) radially along the growth rings, and (3) tangentially along the growth rings (EN 408:2010+A1:2012, 2010). In addition, the microfibril angle varies from species to species, contributing to this variety of material properties (Ramage et al., 2017). As a result, traditional techniques for assessing wood material properties are subject to many uncertainties, making it nearly impossible to distinguish the direction in which the evaluated mechanical properties correspond (Handbook and Wood, 1999).

This work demonstrates an innovative method for feature extraction based on variational mode decomposition (VMD). In this way, ultrasonic bulk waves can be decomposed into some intrinsic mode functions, called IMFs, from which meaningful features can be extracted.

VMD has been used in several applications, including denoising signals used for damage detection (Hassani et al., 2022a,b). This method uses time–frequency domain features derived from ultrasound signals as one of its key features. This implies that the derived features are more likely independent of the distance the ultrasonic wave travels. Thus, regardless of the shape of the specimens, the proposed method is effective at assessing their health.

The analysis of ultrasonic waves using signal decomposition is a reliable approach for gaining information. For example, El Najjar and Mustapha (2021) examined two ultrasound signals obtained from guided ultrasonic tests conducted on wooden poles and identified mode reflections using EEMDAN (ensemble empirical mode decomposition with adaptive noise). In their analysis, the authors concluded that the first four modes of decomposition contained the most information compared to the higher modes (i.e., IMFs 5 to 10). An ultrasound contact test was performed in Mousavi and Gandomi (2021) to determine defects in wooden specimens. VMD was employed to extract descriptive features through three decompositions of an ultrasound bulk wave. The results showed that there are two possible outcomes of VMD's higher modes: the higher mode carries duplicate information or no information at all. Wood inspection using ultrasonic testing was subsequently solved through machine learning algorithms.

This study explores the possibility of using contact–ultrasonics to mechanize the recognition of healthy standing trees for harvesting. Generally, it is imperative to prune trees in time to avoid self-pruning. Trees that have undergone self-pruning are usually found to be knotty and inappropriate for sawlogs (Taskhiri et al., 2020). Therefore, it is essential to hunt such trees down in the field prior to harvesting. Two different experiments, one in the lab and one in the field, were conducted in this study to explore the possibility of using contact–ultrasonic testing to classify wooden specimens into two categories: defective and healthy. Regarding the lab trial, two types of wood specimens, Merbau (*instia palembanica* with a nominal density of 850 kg/m^3) and Pine (Radiata pine or *pinus radiata* with a nominal density of 400 kg/m^3), were studied. In order to synthesize hole-defect in the specimens, two types of holes of varying sizes were drilled into the models; one small and one large. The samples were classified as defective regardless of the size of the hole defects to make the experiment more compatible with the field test. First, some billets were cut from harvested trees at different sites in Collie (WA) and Coffs Harbor (NSW), Australia. Other types of wood were studied at these sites, including Eucalyptus Marginata (Jarrah), Eucalyptus Pilularis (Blackbutt), and Eucalyptus Punctata (Gray gum). The proposed strategy uses the variational mode decomposition (VMD) algorithm to derive descriptive features from the ultrasonic test results conducted on the studied specimens. Next, machine learning and deep learning models were trained to solve the classification problem of the tested samples into two categories, i.e. healthy and defective. This study presents several novel findings, which are listed below:

1. First, the possibility of using VMD as a signal decomposition algorithm for feature extraction from ultrasonic test results is demonstrated by introducing a set of useful features.
2. Since the number of features extracted from the VMD can be specified by the user, a procedure is proposed to select the most appropriate features for solving the classification problems in this paper. Moreover, it was demonstrated that there is quite an overlap between the selected features from the lab and the field's test results.
3. The proposed strategy is further successfully tested on some standing trees in the field by employing trained machine learning and deep learning algorithms.

2. Methodology

2.1. Feature extraction using VMD

Each ultrasonic signal $S(t)$ was first shifted by its mean value and then scaled by the difference between its maximum and minimum values as follows:

$$\overline{\mathbf{S}}(t) = \frac{\mathbf{S}(t) - \mu}{\max(\mathbf{S}(t)) - \min(\mathbf{S}(t))}. \tag{1}$$

where $\overline{S}(t)$ is the normalized version of $S(t)$. The normalized signals were then low-pass filtered with a cutoff frequency of 300 kHz (Mousavi and Gandomi, 2021). The VMD algorithm was employed to derive effective features from the normalized and low-pass filtered ultrasonic signals. Hence, a brief background of VMD theory is presented here to keep the paper self-contained.

VMD solves a variational optimization problem to decompose a nonlinear/non-stationary signal into its constructive modes termed Intrinsic Mode Functions (IMFs). Each IMF is narrow-band and, therefore, can represent only one mode of oscillation of the signal. The general form of the kth IMF is as follows:

$$\mathbf{u}_k(t) = \mathbf{A}_k(t) \cos(\phi_k(t)), \tag{2}$$

where $\mathbf{u}_k(t)$ is the kth IMF with $\mathbf{A}_k(t)$ and $\phi_k(t)$ being its instantaneous amplitude and phase, respectively. The Instantaneous Frequency (IF) of each IMF is obtained as $\omega(t) = \frac{\partial \phi(t)}{\partial t}$. Alternatively, once an IMF is identified, the IF signal can be obtained through Gabor's analytic signal defined as follows (Gabor, 1946):

$$\mathbf{u}_a(t) = \mathbf{u}(t) + j\hat{\mathbf{u}}(t), \tag{3}$$

where $\mathbf{u}_a(t)$ is the Gabor's analytic signal, j is the imaginary unit, and $\hat{\mathbf{u}}(t)$ is the Hilbert transform (Muskhelishvili and Radok, 2008) of the given IMF signal $\mathbf{u}(t)$. As such, the instantaneous frequency of the IMF is obtained as follows:

$$\omega(t) = \frac{\mathrm{d}}{\mathrm{d}t}\left(\tan^{-1}\left(\frac{\hat{\mathbf{u}}(t)}{\mathbf{u}(t)}\right)\right), \tag{4}$$

The following procedures are followed to construct the variational optimization problem of the VMD:

Step (1): First, the unilateral Hilbert transform of the kth IMF is obtained as $\left(\delta(t) + \frac{j}{\pi t}\right) * \mathbf{u}_k(t)$, where δ, j, and $*$ denote the Dirac distribution, the imaginary unit, and the convolution operator, respectively.

Step (2): A center frequency ω_k is assumed for the kth IMF, and the obtained Hilbert spectrum from step (1) is shifted to the baseband as $\left[\left(\delta(t) + \frac{j}{\pi t}\right) * \mathbf{u}_k(t)\right] \times e^{-j\omega_k t}$.

Step (3): Then, the squared L^2 norm of the gradient of the shifted spectrum from step (2) is calculated as $\left\|\partial_t\left[\left(\delta(t) + \frac{j}{\pi t}\right) * \mathbf{u}_k(t)\right] \times e^{-j\omega_k t}\right\|^2$.

Step (4): Finally, the L^2 norm of the gradients is summed over all IMFs to construct the conditional optimization problem of the VMD, on $\mathbf{u}_k$ and ω_k, as follows:

$$\min_{\mathbf{u}_k \& \omega_k} \sum_k \left\|\partial_t\left(\delta(t) + \frac{j}{\pi t} * \mathbf{u}_k(t)\right) \times e^{-j\omega_k t}\right\|_2^2, \ s.t. \ \mathbf{f}(t) = \sum_k \mathbf{u}_k(t) \tag{5}$$

where the sum of the obtained IMFs constructs the original signal minus some noise depending on the settings.

The following alternative Lagrangian is constructed to solve the optimization problem of (5), (Dragomiretskiy and Zosso, 2014):

$$\mathcal{L}(\mathbf{u}_k, \omega_k, \lambda) = \alpha \sum_k \left\|\partial_t\left(\delta(t) + \frac{j}{\pi t} * \mathbf{u}_k(t)\right) \times e^{-j\omega_k t}\right\|_2^2$$

Table 1
VMD parameters.

Parameters	Description	Specified values
p	Number of IMFs	3
α	Denoising factor	N.A.
τ	Time interval	0.1
ϵ	Convergence threshold	10^{-5}
$init$	Center frequency initializer	0
DC	Boolean parameter	0

Table 2
The description of all features naming.

Features	Description	Features	Description
x_1	ω of IMF$_1$	x_{12}	$Q1_{\mathrm{IF}}$ of IMF$_2$
x_2	RMS$_{\mathrm{IF}}$ of IMF$_1$	x_{13}	$Q2_{\mathrm{IF}}$ of IMF$_2$
x_3	ω of IMF$_2$	x_{14}	$Q3_{\mathrm{IF}}$ of IMF$_2$
x_4	RMS$_{\mathrm{IF}}$ of IMF$_2$	x_{15}	k_{IF} of IMF$_2$
x_5	ω of IMF$_3$	x_{16}	σ_{IF} of IMF$_2$
x_6	RMS$_{\mathrm{IF}}$ of IMF$_3$	x_{17}	$Q1_{\mathrm{IF}}$ of IMF$_3$
x_7	$Q1_{\mathrm{IF}}$ of IMF$_1$	x_{18}	$Q2_{\mathrm{IF}}$ of IMF$_3$
x_8	$Q2_{\mathrm{IF}}$ of IMF$_1$	x_{19}	$Q3_{\mathrm{IF}}$ of IMF$_3$
x_9	$Q3_{\mathrm{IF}}$ of IMF$_1$	x_{20}	k_{IF} of IMF$_3$
x_{10}	k_{IF} of IMF$_1$	x_{21}	σ_{IF} of IMF$_3$
x_{11}	σ_{IF} of IMF$_1$	–	–

$$+ \left\|\mathbf{f}(t) - \sum_k \mathbf{u}_k(t)\right\|_2^2 + \left\langle \lambda(t), \mathbf{f}(t) - \sum_k \mathbf{u}_k(t) \right\rangle \tag{6}$$

This makes the VMD a parametric decomposition algorithm, requiring its parameters to be specified in computer program settings before running the decomposition algorithm (Zosso, 2020). In this study, the parameters of the VMD and the values selected for each are listed in Table 1. For further details about specifying the parameters, readers are referred to Mousavi and Gandomi (2021). The signal was set to be decomposed into three IMFs based on the results of Mousavi and Gandomi (2021). Accordingly, more decompositions can result in having duplicated IMFs in higher-order IMFs (IMFs with higher center frequency), which will compromise the effectiveness of the extracted features and ML results.

Seven types of features were selected for each IMF as follows:

1. The center frequency of the IMF (ω).
2. The Root Mean Square (RMS) of the IF signal, obtained for the IMF as follows (Mousavi and Gandomi, 2021):

$$\mathrm{RMS}_{\mathrm{IF}} = \sqrt{\frac{\sum_{i=1}^n \omega(t)^2}{n}}, \tag{7}$$

where RMS$_{\mathrm{IF}}$ is the root mean square of the IF signal $\omega(t)$, and n is the length of the signal.

3. The first quartile of the IF signal, shown as $Q1_{\mathrm{IF}}$, indicates the value under which 25% of IF points are located when arranged in ascending order.
4. The second quartile of the IF signal or the median, shown as $Q2_{\mathrm{IF}}$, indicates the value under which 50% of IF points are located when arranged in ascending order.
5. The third quartile of the IF signal, shown as $Q3_{\mathrm{IF}}$, indicates the value under which 75% of IF points are located when arranged in ascending order.
6. The variance of the IF signal, shown as σ_{IF}.
7. The Kurtosis of the IF signal, shown as k_{IF}.

Therefore, there is a total of 21 features derived for each test result, named from x_1 to x_{21} as shown in Table 2.

2.2. Feature selection

It is essential to select the most practical features for training the MLAs in order to, first, avoid using uncorrelated features that will only
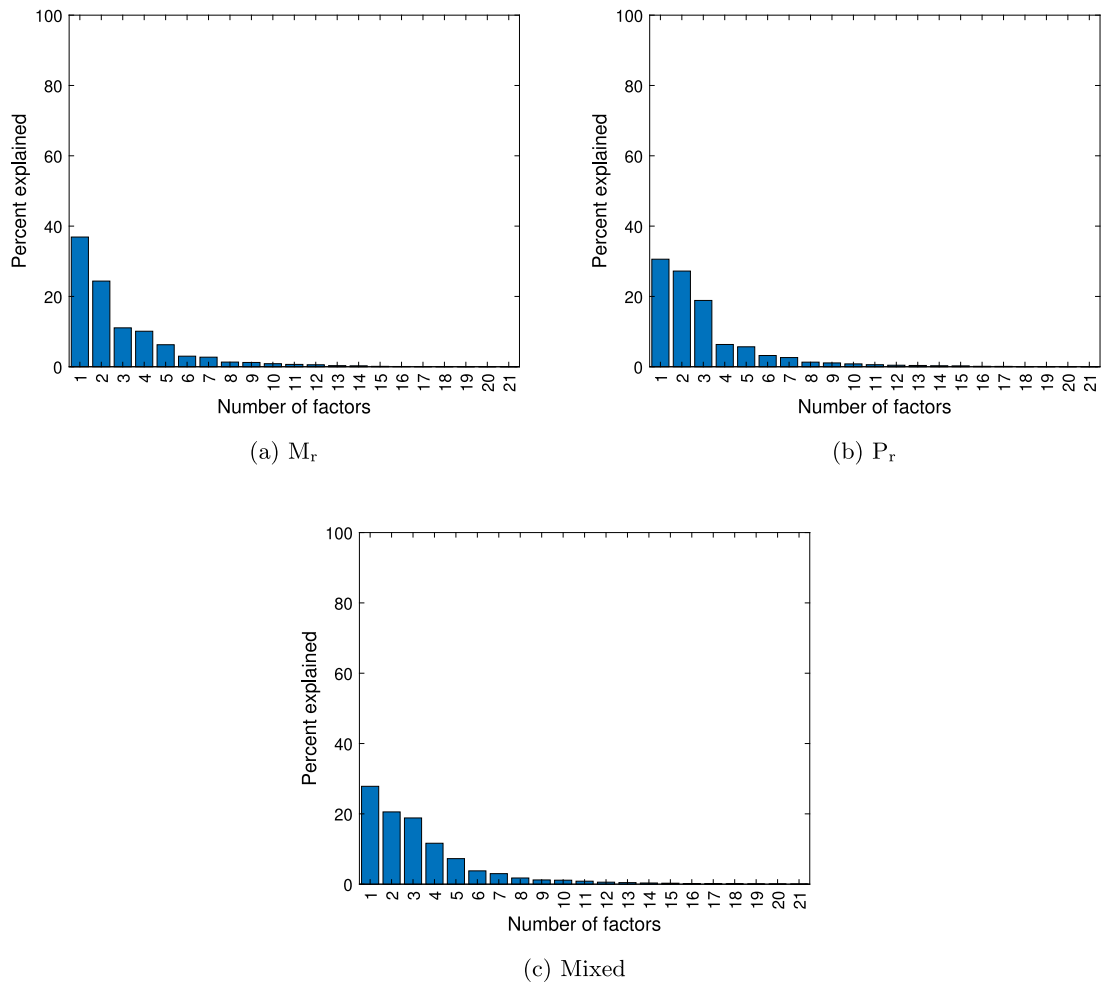
(a) M_r

(b) P_r

(c) Mixed

Fig. 1. Scree plots of the PCA applied to the dataset corresponding to the (a) M_r, (b) P_r, (c) mixed observations.

increase the time of the training process and, secondly, prevent over-fitting of the model on the training dataset, which will consequently increase the variance between the test set and training set accuracy. To this end, principal component analysis (PCA) is employed to explore the importance of each feature. Generally, the most important features are more correlated with lower order PCs, i.e. PC_1 and PC_2, and components that are not correlated with the lower order PCs are less critical in describing the variability of the dataset across different observations.

Consider the standardized[1] feature matrix $\mathbf{X}_{m \times p}$ of rank $r \leq \min\{m, p\}$, that has the obtained features per observation stacked up in its rows. The singular value decomposition of $\mathbf{X}$ is written as follows:

$$\mathbf{X} = \mathbf{P}\Delta\mathbf{Q}^{\mathrm{T}}, \tag{8}$$

where $\mathbf{P}_{m \times r}$ and $\mathbf{Q}_{p \times r}$ are matrices of left singular and right singular vectors, respectively. Note that $\mathbf{Q}$ is a unitary matrix, i.e. $\mathbf{Q}^{-1} = \mathbf{Q}^{\mathrm{T}}$. Finally, the diagonal matrix of singular values is obtained as $\Delta_{r \times r}$. The principal components of $\mathbf{X}$ are stacked up in the columns of the matrix of factor scores, $\mathbf{F}$, obtained as follows:

$$\mathbf{F} = \mathbf{P}\Delta, \tag{9}$$

whose columns represent the projected observations on the principal axes. Since $\mathbf{Q}$ is a unitary matrix, one can write:

$$\mathbf{F} = \mathbf{P}\Delta = \mathbf{P}\Delta\mathbf{Q}^{\mathrm{T}}\mathbf{Q} = \mathbf{X}\,\mathbf{Q}. \tag{10}$$

Therefore, $\mathbf{Q}$ can also be interpreted as a projection matrix. As such, the contribution of a component to a variable called "loading" is obtained from the calculation of the squared entries of $\mathbf{Q}$. Hence, the rows of $\mathbf{Q}^2$ correspond to the loading of variables evaluated in the principal direction of each column. In order to select the most compelling features for classification, we propose the following procedure to be followed:

1. Obtain the variance percentage explained by each PC corresponding to the standardized feature matrix X.
2. Multiply the variance percentage of the PC to the corresponding column of the $\mathbf{Q}^2$.
3. Sum the results of step (2) over the selected PCs. Note that one may choose to determine the number of PCs based on the accumulated variance explained by them. However, the first three PCs were selected in this study in all cases.

The above concept can be written in the form of an equation as follows:

$$\mathbf{I} = \sum_{i=1}^{N} var(i) \times \mathbf{Q}^2(:, i) \tag{11}$$

where $\mathbf{I}$ is a vector of the obtained importance value for each feature, N is the number of selected PCs, $var(i)$ represents the amount of variance explained by the ith PC, and $N = 3$.
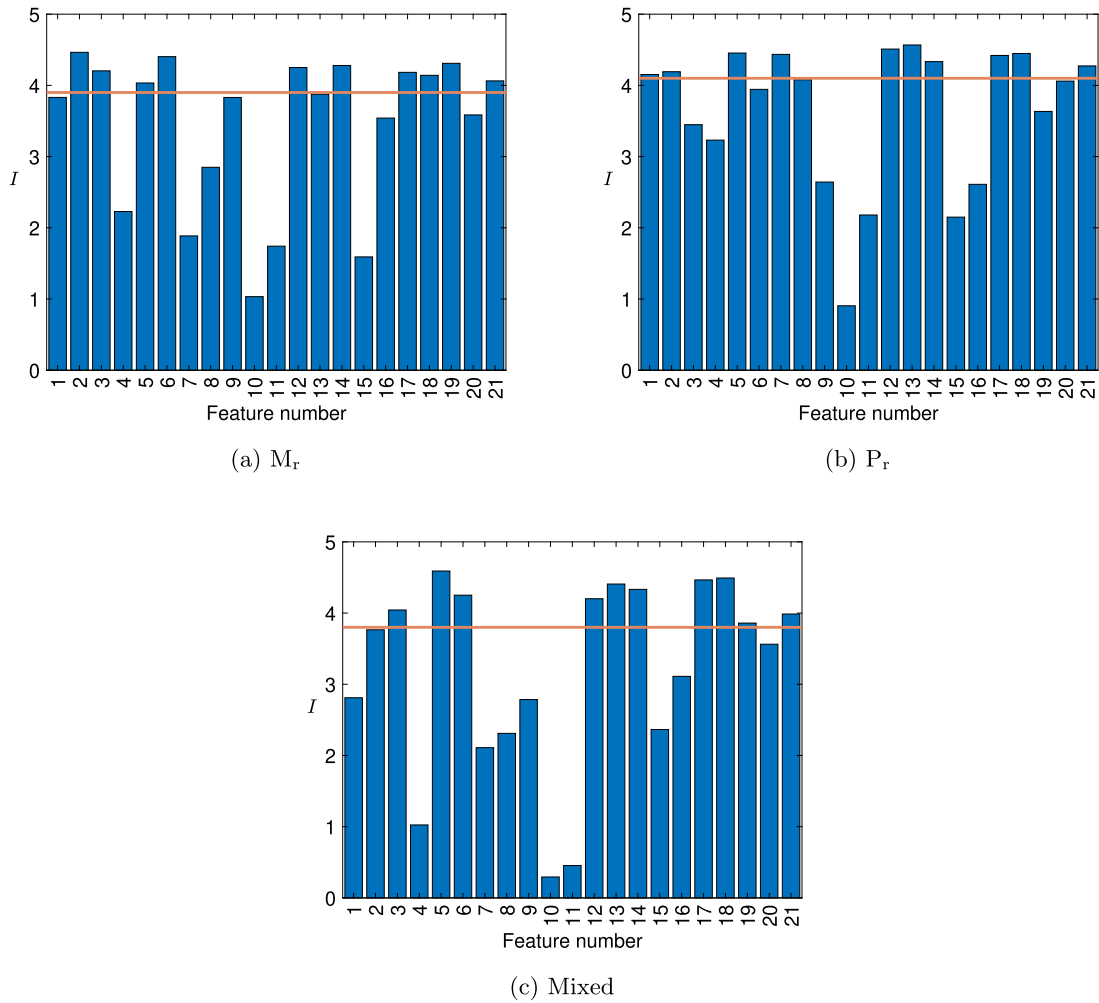
---

[1] The standardized matrix $\mathbf{X}$ is obtained through centering each of its columns concerning the mean value of all the observations in that column divided by their standard deviation.

(a) M_r

(b) P_r

(c) Mixed

Fig. 2. Contribution percentage of each feature to the first principal dimension for (a) M_r, (b) P_r, (c) mixed observations.

Table 3
MLAs employed for solving the classification problems.

Trees	Discriminant	Naive Bayes	SVM	Nearest neighbor	Ensemble
Fine	Linear	Gaussian	Linear	Fine	Boosted trees
Medium	Quadratic	Kernel	Quadratic	Medium	Bagged trees
Coarse	–	–	Cubic	Coarse	Subspace discriminant
–	–	–	Fine Gaussian	Cosine	Subspace KNN
–	–	–	Medium Gaussian	Cubic	RUSBoosted trees
–	–	–	Coarse Gaussian	Weighted	–

2.3. Employed machine learning algorithms

The machine learning toolbox in MATLAB was exploited to solve the classification problems in this study. The MLAs employed for solving the classification problems are listed in Table 3.

3. Lab trial results

In this section, the problem of wood hole-defect classification in two types of wood, i.e. Merbau (hardwood) and Pine (softwood), is solved. The problem of this section is mainly set to serve as a controlled lab trial for classifying wood with natural imperfections in the field. The specifications of the test set-up are listed in Table 4. The dimensions of the specimens were $90 \times 90 \times 300$ mm^3. There were two types of defects implemented on the specimens: (1) a small hole with a diameter of 6 mm (7% of the cross-section) and (2) a larger hole with a diameter of 13 mm (14% of the cross-section). The hole damage was drilled

into the radial cross-sections. As for the weather conditions within the room during testing, there were moderate fluctuations in temperature, ranging from 20–22 °C. It was about 60% humidity on average. There were no significant differences between lab specimens in terms of moisture levels (usually ten to fifteen percent, depending on the locale's climate) (Mousavi et al., 2020). A Pundit PL200 was used for ultrasonic testing (Fig. 3(b)), where a 54 kHz transducer was used to transmit a sinc-like probing P-wave (compression wave) with a pulse repetition frequency (PRF) of 5 Hz. During operation, the device generates 17.5 μs sinc-like impulses. According to the manual: "transducers supplied with the instrument are not damped and, therefore, on being excited by the transmitter, they have a long ring-down time". As a result, it is possible to assume that the signal transmitted into the sample is a lightly damped impulse response. Due to the lower repetition frequency of pulses than the resonant frequency of the transducer, pulses do not mix. A limited number of frequencies can be selected for use with the Pundit PL200, which must match the frequency of the selected transducer pair. For the current work, the receiver gain was set to the device's '1 dB'

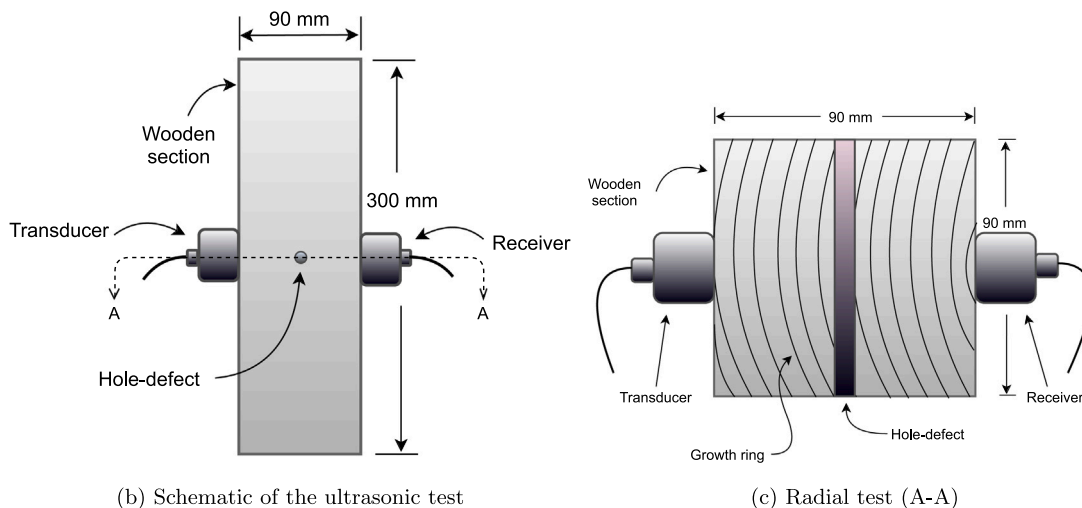(a) Ultrasonic device (Pundit PL 200)(Mousavi et al., 2020)

(b) Schematic of the ultrasonic test

(c) Radial test (A-A)

Fig. 3. Ultrasonic test experimental set-up.

Table 4
Technical specifications of the test set-up.

Ultrasonic device	Pundit PL200
Prob frequency	54 kHz
Sampling frequency	10 MHz
Couplant gel	Proceq Ultraschall-Koppelpaste

Table 5
The number of test samples collected from different types of wood through ultrasonic tests.

Radial test (tangential defect)			
Defect type	Specimens #	Pine test #	Merbau test #
Intact	6	300	300
Small tangential defect	3	150	150
Large tangential defect	3	150	150

setting. Several trial runs were conducted to ensure the signal is strong but not saturated. Probe waves are P-waves (compressional waves), with transducer voltages of 50 V.

By interacting with wood irregularities, the receiver recorded modulated ultrasonic waves at a sampling frequency of 10 MHz as recommended in other works, including (Nasir et al., 2021). To ensure the effective transmission of ultrasonic waves into and out of the wood samples, couplant gel (Proceq Ultraschall-Koppelpaste) was applied between the transducer/receiver and the wood surface.[2]

The contact–ultrasonic testing is sensitive to the following items:

1. The amount of the coupling gel applied to the surface of the wood at the transducer and receiver sides.
2. Any vibration of the hands upon testing while holding the transducer and receiver.
3. The amount of pressure applied to the transducer and receiver.

Therefore, 50 replicates of the ultrasonic tests were conducted on each specimen. Table 5 shows the number of tests performed on the samples' different types and health conditions.

Two classes were considered in this study: (1) healthy and (2) defective. As such, small and large damage is classified as defective. This is mainly because the size of the defect is not a factor in standing tree inspection. Therefore, this was done primarily to align with the field
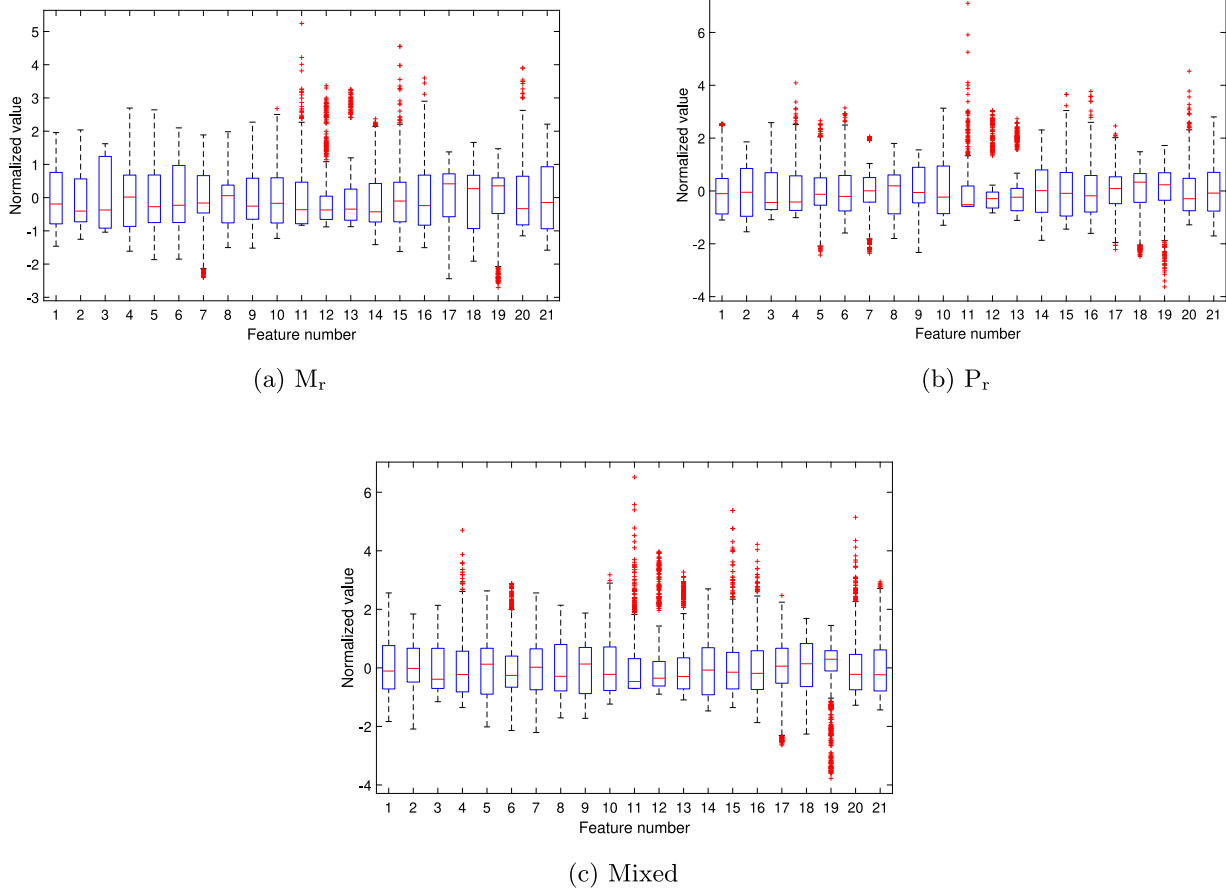
---

[2] For further details, readers are referred to Mousavi and Gandomi (2021) and Mousavi et al. (2020).

(a) M_r

(b) P_r

(c) Mixed

Fig. 4. Box plot of the standardized features regarding (a) M_r, (b) P_r, and (c) mixed observations.

trials section. Fig. 4 showcases the box plot of standardized features for (a) M_r (Fig. 4(a)), (b) P_r (Fig. 4(b)), and (c) mixed observations (Fig. 4(c)). The middle red line indicates the median of the feature distribution. The lower and upper bounds of the box correspond to the first (Q_1) and third (Q_3) quartiles regarding the distribution of the feature, respectively. The range between (Q_1) and (Q_3) denotes the interquartile range (IQR). The lower and upper whiskers correspond to the minimum of $Q_1 - 1.5 \times$ IQR and the maximum of $Q_3 + 1.5 \times$ IQR that the feature can take. Observations outside the defined ranges are shown with a + sign and correspond to outliers. The median located at the center of the box coincides with the mean, indicating the feature distribution is symmetric. However, the median located below and above the centerline of the box indicates that the feature distribution is right- and left-skewed, respectively. As such, the box plot of different features suggests several features for each case follow an asymmetric distribution. Moreover, multiple features have values that can be considered outliers.

From the box plots of features extracted from test results in the lab, the following conclusions can be drawn:

1. Features are spread, showing the diversity of the test result by replicating the experiment, where in some cases, out-of-distribution value for attributes is evident.
2. Most features follow asymmetrical distribution, indicating that the value of features occurs at irregular frequencies.
3. The existence of outliers again indicates how loosely the data is grouped and therefore, the application of machine learning algorithms is well justified.

Fig. 5 shows the scatter plot of PC_1 versus PC_2 of the standardized feature space regarding (a) M_r (Fig. 5(a)), (b) P_r (Fig. 5(b)), and (c)

mixed observations (Fig. 5(c)). As can be seen from the scatter plots, it is not straightforward to separate the classes.

The MLAs listed in Table 3 have been used to answer the following questions:

1. Do the selected features capture enough variability in the obtained ultrasonic signals across different specimens?
2. How will the trained MLAs perform on a mixture of different types of wood?

Fig. 1 shows the Scree plots of different types of specimens and a mixture of them. It can be seen that the amount of variance explained by higher-order PCs is always smaller than those described by lower-order PCs. Therefore, it is reasonable to select only the three first columns of the $\mathbf{Q}^2$ corresponding to the first three PCs in (11). As such, the plots of Fig. 2 are obtained that describe the contribution of each feature to the variability of the feature space across different observations when the observations from different types of wood are considered individually or mixed. A threshold was set for the value of entries in vector **I** for each case to pick the first ten most effective features for training. Table 6 shows the selected features for different types of wood based on their correlation with the first three PCs. As can be seen from the table, features $x_{21}, x_{18}, x_{17}, x_{14}, x_{12}$, and x_5 are recognized as the most effective in all cases.

Table 7 shows the 5-fold cross-validation accuracy results obtained from various MLAs trained on each type of wood and their mixture. The results indicate that the "Fine Gaussian SVM" is the most effective algorithm for the classification of all three problems, i.e. M_r, P_r, and their mixture with the accuracy index of 100, 100, and 99.9 percent, respectively. The other observation is that the accuracy slightly declines in most cases of using different MLAs when the samples are mixed.
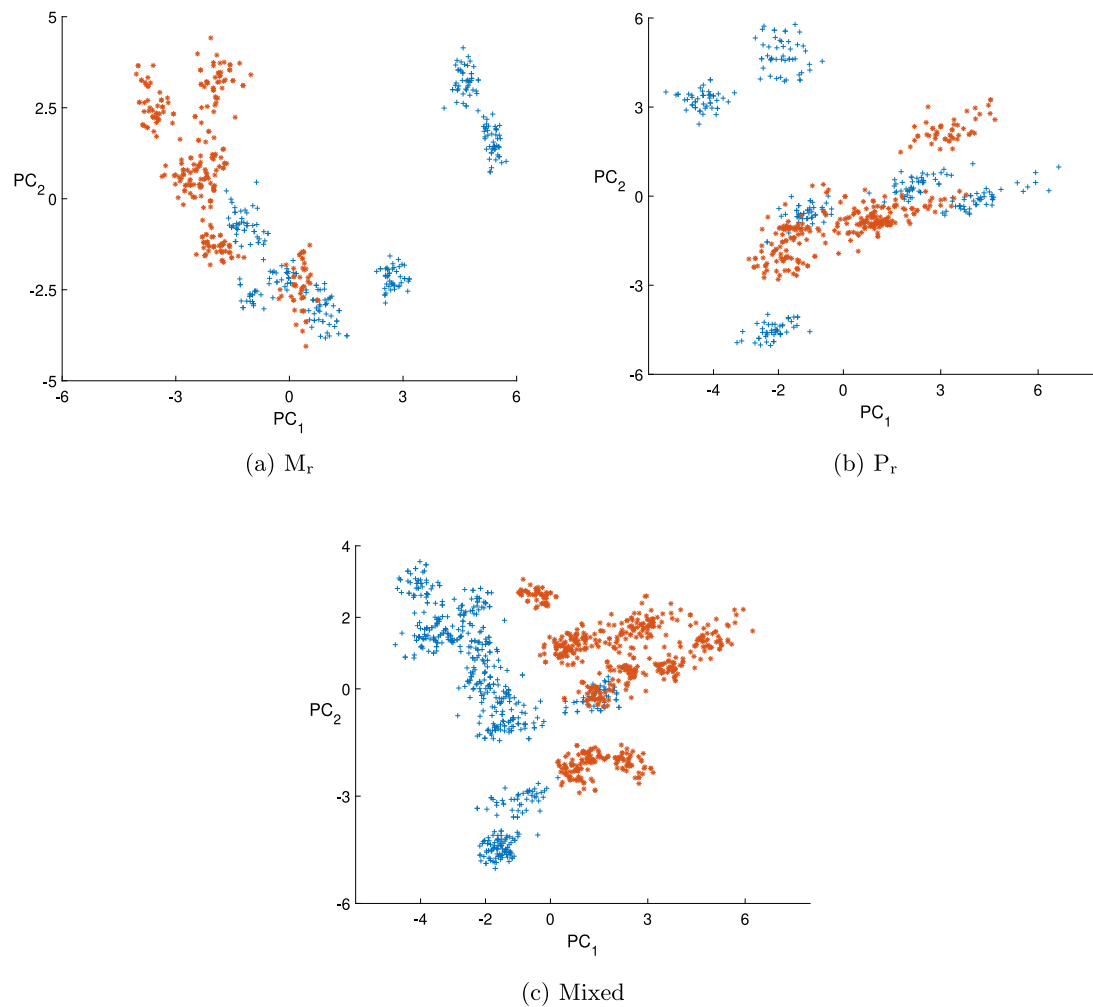
(a) M_r

(b) P_r

(c) Mixed

Fig. 5. Scatter plot of PC_1 versus PC_2 of the standardized feature space regarding (a) M_r, (b) P_r, and (c) mixed observations.

Table 6
VMD parameters.

Type of wood	Selected features
M_r	$x_{21}, x_{19}, x_{18}, x_{17}, x_{14}, x_{12}, x_6, x_5, x_3, x_2$
P_r	$x_{21}, x_{18}, x_{17}, x_{14}, x_{13}, x_{12}, x_7, x_5, x_2, x_1$
Mixture	$x_{21}, x_{19}, x_{18}, x_{17}, x_{14}, x_{13}, x_{12}, x_6, x_5, x_3$

Table 7
The classification results of different MLAs applied to the lab test results.

MLA	M_r	P_r	Mixed
Fine trees	98.5	100	97.8
Medium trees	98.5	100	97.8
Coarse trees	97.8	100	89.1
Linear discriminant	97.5	100	86.1
Quadratic discriminant	100	100	88.8
Gaussian Naïve Byes	81.8	98.7	80.3
Kernel Naïve Byes	95.3	100	84.4
Linear SVM	100	100	87.5
Quadratic SVM	100	100	97.9
Cubic SVM	100	100	99.4
Fine Gaussian SVM	100	100	99.9
Medium Gaussian SVM	100	100	96
Coarse Gaussian SVM	90.2	100	80.4
Fine nearest neighbor	100	100	99.8
Medium nearest neighbor	100	100	99.6
Coarse nearest neighbor	87.7	96.2	82.9
Cosine nearest neighbor	100	100	99.3
Cubic nearest neighbor	100	100	99.5
Weighted nearest neighbor	100	100	99.8
Boosted trees	50	50	50
Bagged trees	99.8	100	99.3
Subspace discriminant	92.5	100	81
Subspace KNN	100	100	99.8
RUSBoosted trees	50	50	50

4. Field experimental results

4.1. Using machine learning

In this section, the problem of classification of standing trees based on no defect in their trunk is studied. This problem has been given much attention due to its importance in facilitating the mechanized harvesting process. If trees with natural imperfections are appropriately identified, they will not be subjected to sawing. This is vital as the bulk of timber with natural defects is usually sold as pulpwood.

Multiple specimens from different types of wood at various sites in Western Australia (WA) and New South Wales (NSW) were tested using the Pundit PL-200 ultrasonic device. Table 8 shows the types of wood and the environmental conditions at each site upon which the tests were conducted. As such, there was one type of wood (Jarrah) tested at the WA site (Collie) and two different types of wood, namely Blackbutt and Greygum, tested at the NSW site (Coffs Harbor). All of these spices, however, are classified as members of the Eucalyptus family. The temperature in the WA and NSW sites was respectively

Fig. 6. All trees were visually inspected and marked with spray marker.

Table 8
Wood from different sites with different meteorological condition were tested.

State	Site	Wood species	Temperature (°C)	Humidity (%)
WA	Collie	Jarrah	5.1	90
NSW	Coffs harbor	Blackbutt & Greygum	10	90

Table 9
The number of billets and ultrasonic tests conducted on woods of different sites.

Number of billets		
Condition	WA #	NSW #
Intact	37	7
Defective	37	28
Number of ultrasonic test		
Condition	WA #	NSW #
Intact	838	213
Defective	897	617

5.1 and 10 degrees Celsius, while the relative humidity in both was almost 90 percent. The average moisture content of standing trees in the winter climate of both sites was around 90%. Previous experiences indicate that defects usually appear at the minimum breast height of a standing tree. Therefore, some billets between breast height and the highest commercial elevation of the corresponding standing trees were harvested and further tested. The breast height was roughly 1.3 m above the highest point of the ground at the base of the tree. The length of the billets was 20 cm each.

Table 9 shows the number of billets from each site and the overall number of ultrasonic tests conducted on them. Likewise, in the lab trial section, there were two labels assigned to the tested specimens, namely healthy and defective, which were specified through visual inspection. The woods were tested in different randomly selected directions based on how flat the surface of the tested tree was. All specimens were debarked at the point of testing using a hammer. The billets were

harvested from 6 standing trees of each species. All trees were visually inspected and marked with a spray marker, as shown in Fig. 6.

The obtained ultrasonic test results were preprocessed using the VMD algorithm to derive the required features, as discussed in Section 2.1. Fig. 7 showcases the box plot of standardized features for sites in (a) WA (Fig. 7(a)), (b) NSW (Fig. 7(b)), and (c) mixed observations (Fig. 7(c)). The same observations as those in the lab trial sections are evident from the boxplots of this section. It can be seen that, in this case, the number of outliers is even larger, indicating that the data
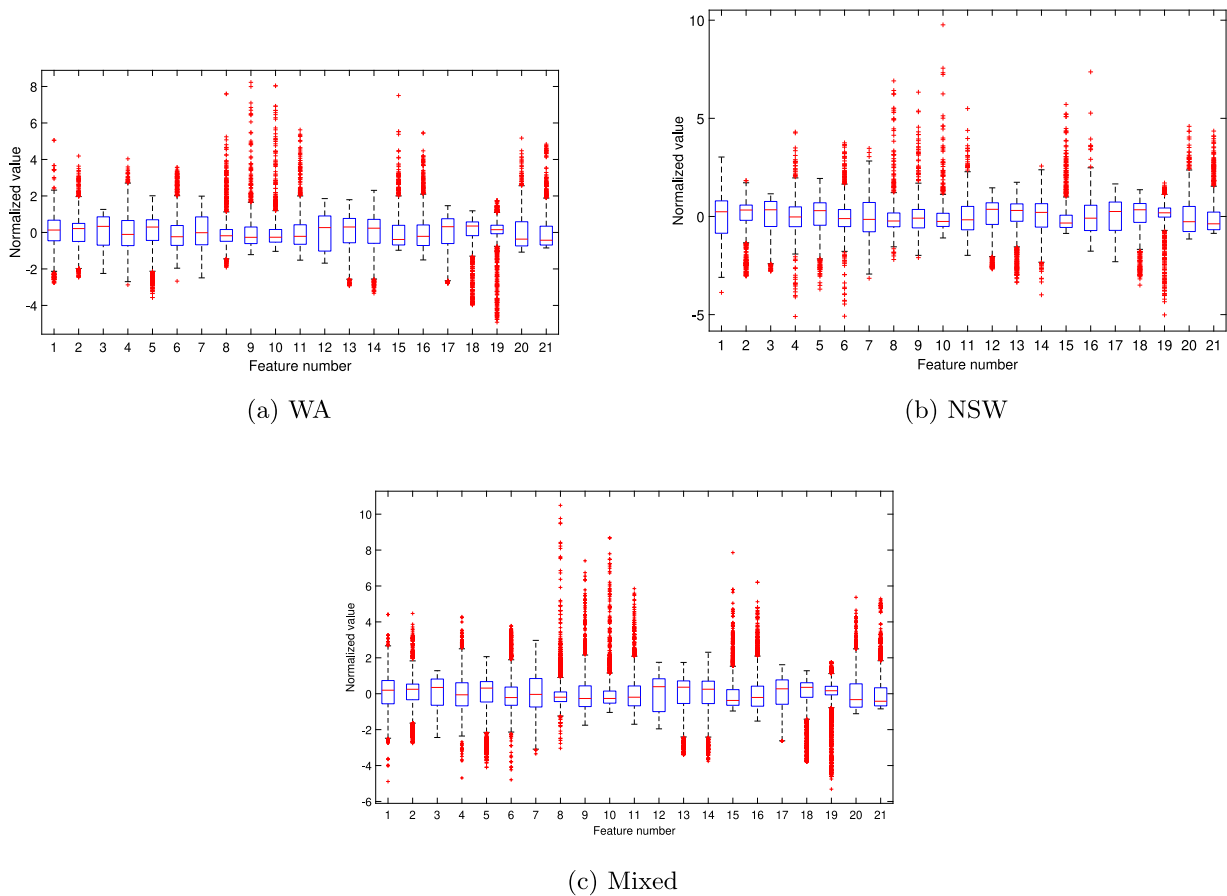
(a) WA

(b) NSW

(c) Mixed

Fig. 7. Box plot of the standardized features obtained from test data collected from billets at sites (a) WA, (b) NSW, and (c) mixed observations.

is not tightly grouped. There are several reasons for that, such as the following:

1. Testing the billets in different directions yields different results due to the characteristic of the wood being an orthotropic material.
2. The testing conditions can be affected by those uncertainties in the lab trial justifying the diversity of the test results.
3. The billets are not perfectly cylindrical, meaning that the ultrasound wave travels different distances when transmitted through different angles.

Fig. 8 showcases PC_1 versus PC_2 of the standardized feature space regarding tested billets from (a) WA (Fig. 8(a)), (b) NSW (Fig. 8(b)), and (c) mixed observations from both sites (Fig. 8(c)). Although the plots show a degree of separability of the classes in all three cases, the problem is predicted to be more challenging compared to the lab trial experiments.

The Scree plot of the PCA algorithm applied to the standardized X was first obtained, as shown in Fig. 9, to select the most compelling features for training. Then, the variance explained by the first three PCs was used to obtain the effectiveness of features through (11). The contribution of features to the variability of the dataset pertaining to the specimens tested in WA, NSW, and their mixture is presented in Fig. 10. Next, a threshold was set for each case to select the ten most useful features, as listed in Table 10. As can be seen from the table, features $x_{21}, x_{18}, x_{17}, x_{13}, x_{12}, x_7, x_4$, and x_2 were identically selected among the most effective features in all cases. This also has an overlap with the most effective features selected for the lab trial cases, which are x_{21}, x_{18}, x_{17}, and x_{12}.

Next, the MLAs of Table 3 were employed to solve the classification problem of billets based on their health state in different states. Interestingly, similar to the lab trial results, the Fine Gaussian SVM performs

Table 10
Selected features for each type of wood in different states and a mixture of them.

Type of wood	Selected features
WA	$x_{21}, x_{18}, x_{17}, x_{14}, x_{13}, x_{12}, x_7, x_5, x_4, x_2$
NSW	$x_{21}, x_{18}, x_{17}, x_{13}, x_{12}, x_9, x_8, x_7, x_4, x_2$
Mixture	$x_{21}, x_{18}, x_{17}, x_{14}, x_{13}, x_{12}, x_7, x_5, x_4, x_2$

best on all cases of WA, NSW, and a mixture of them with a 5-fold cross-validation accuracy of 93.9, 96.7, and 94 percent, respectively (see Table 11).

4.2. Using deep learning

Thus far, the results of applying conventional MLAs for solving the classification problem of billets were presented and discussed. However, deep learning architectures have been widely used to solve problems in different fields. Different architectures of deep convolutional neural networks can be found in Khan et al. (2020). In this section, a one-dimensional Convolutional Neural Network (1D-CNN) is developed that takes the identified practical features from the previous sections as input and outputs the class of billets as healthy or defective. The architecture of the employed 1D-CNN is depicted in Fig. 11. Some essential parameters in the employed 1D-CNN are as follows: learning rate was initially set at 0.01 and was assigned to drop at every 200 epochs with a dropping rate of 0.5; momentum was 0.9; mini-batch size was set at 128; the total epoch number was set at 1000. The damage identification results of the 1D-CNN are presented in Table 12. Table 12 shows the results of the 5-fold cross-validation accuracy for the training and test sets. The results indicate the better performance of the trained 1D-CNN model on billets harvested from NSW sites. This is ideally in
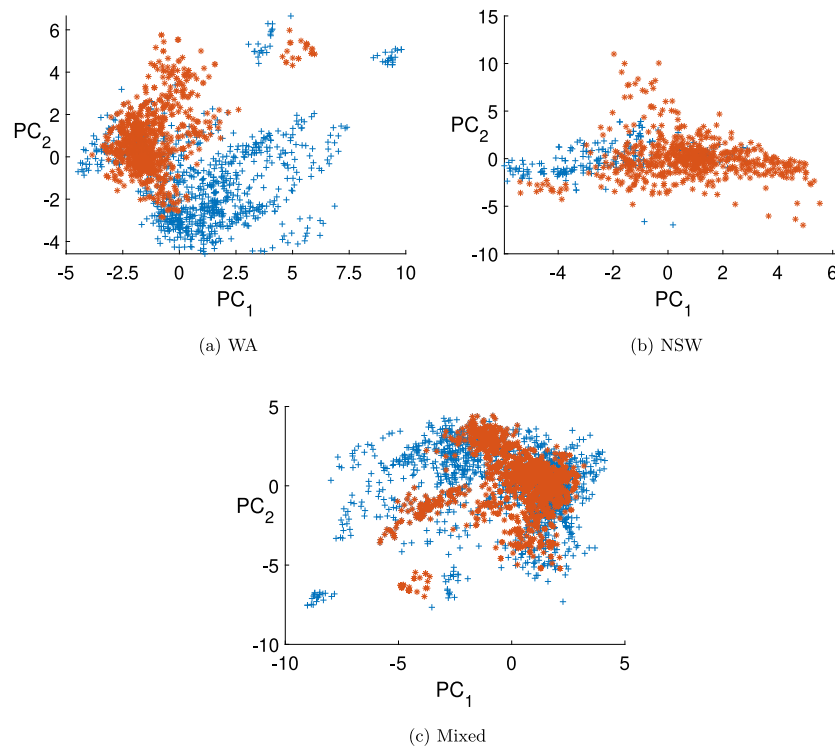
(a) WA

(b) NSW

(c) Mixed

Fig. 8. Scatter plot of PC_1 versus PC_2 of the standardized feature space regarding tested billets from (a) WA, (b) NSW, and (c) mixed observations.

Table 11
The classification results of different MLAs applied to the field test results.

MLA	WA	NSW	Mixed
Fine trees	91.2	94.1	90.3
Medium trees	91.0	94.5	89.8
Coarse trees	88.2	90.6	85.2
Linear discriminant	88.0	90.1	85.7
Quadratic discriminant	87.5	91.3	85.7
Gaussian Naïve Byes	85.4	84.5	82.2
Kernel Naïve Byes	87.5	86.7	85.3
Linear SVM	90.4	91.9	86.8
Quadratic SVM	93.2	95.4	91.6
Cubic SVM	91.8	95.4	92.2
Fine Gaussian SVM	93.9	96.7	94
Medium Gaussian SVM	93.3	95.2	91.7
Coarse Gaussian SVM	90.4	90.4	87.1
Fine nearest neighbor	91.2	94.8	91.5
Medium nearest neighbor	93.5	95.3	92.9
Coarse nearest neighbor	88.0	87.5	85.7
Cosine nearest neighbor	92.2	93.6	91.8
Cubic nearest neighbor	93.5	94.9	92.8
Weighted nearest neighbor	93.3	95.9	94.1
Boosted trees	92.7	94.9	92
Bagged trees	93.3	96.4	93.3
Subspace discriminant	86.6	90.1	85.2
Subspace KNN	91.5	96.5	92.2
RUSBoosted trees	91.9	95.5	90.7

Table 12
The 5-fold cross-validation accuracy results obtained for the training and test sets using the trained 1D-CNN models with selected features.

Accuracy (%)	WA	NSW	Mixed
Training	96.3	99.7	97.8
Testing	92.5	96.3	92.2

deep models. However, the main reason here to train 1D-CNN models with and without feature selection was to further assess the power of the proposed feature selection algorithm. Tables 12 and 13 show the variance between training and testing accuracy in both cases. The variance between the accuracy results of the 1D-CNN model with selected features on data collected from WA, NSW, and Mixed samples yielded 3.8, 3.4, and 5.6 percent, respectively. Likewise, the results obtained for the 1D-CNN model with all features on data collected from WA, NSW, and Mixed samples returned 5, 2.3, and 4.8 percent, respectively. Comparing the results indicates that while the performance of the model on WA samples improved, its performance slightly worsened for the NSW and Mixture samples. However, these improvements are marginal and can be overlooked. As such, the validity of the feature selection algorithm is confirmed.

The proposed procedure is meant to be independent of the type of wood on which the model is trained. We have checked this hypothesis by mixing test results obtained from different types of wood and an acceptable accuracy ranges were achieved. For example, the results of Tables 12 and 13 show that not only mixing different types of wood in WA and NSW did not compromise the effectiveness of the model in Table 12, but also improved the performance of the model in Table 13.

5. Further testing the trained models

Thus far, the results of solving the classification problem of billets have been presented and discussed. To further assess the capability of the trained models in identifying defective and healthy trees, several
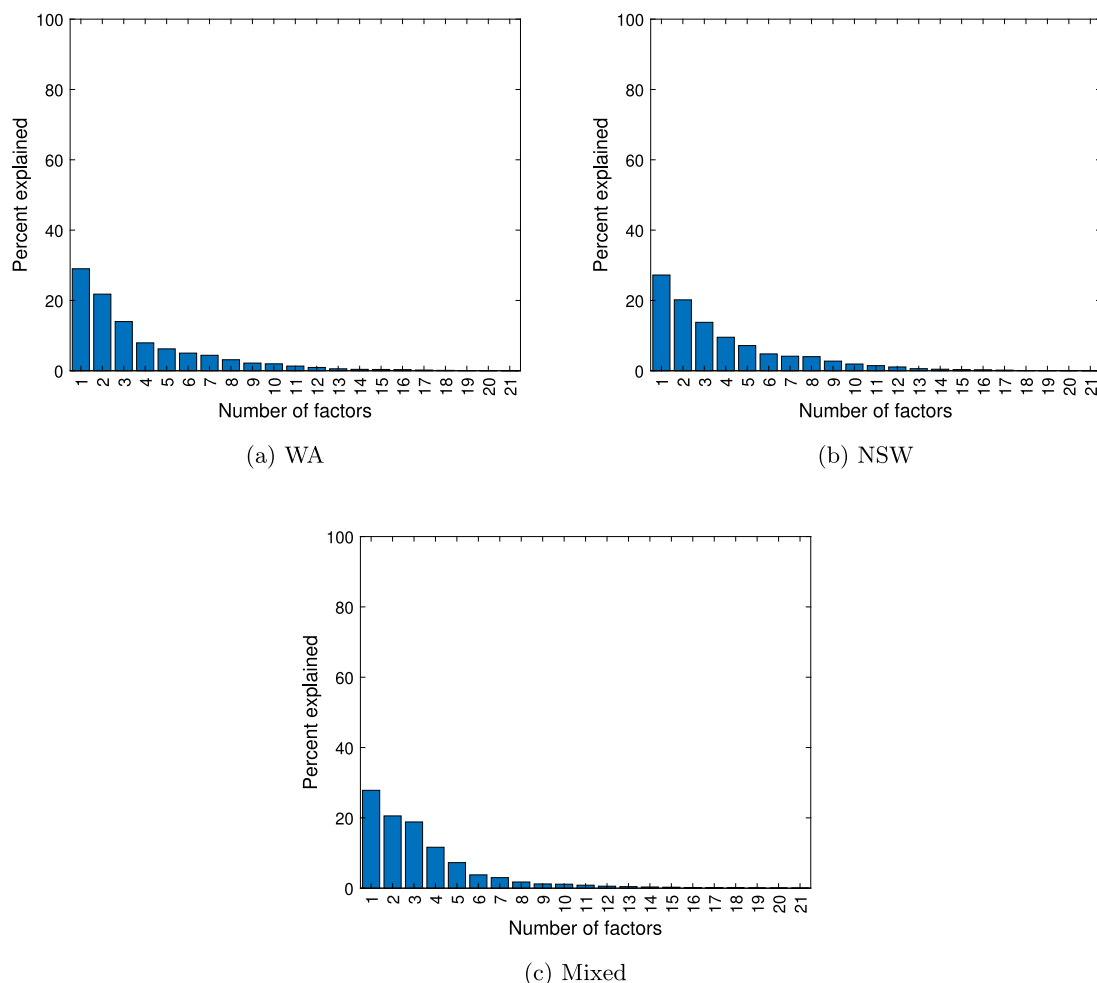
line with the results obtained through ML algorithms. Next, the trained models are further tested on data collected from testing some standing trees.

To highlight the effect of feature selection on training the 1D-CNN models, all features are next introduced to the models for training. Table 13. The results show less variance for the model trained on WA specimens with selected features compared to all features. Opposite conclusions can be drawn for models trained on NSW and Mixed specimens, although the difference is still marginal.

It is not typical to perform feature selection prior to running a CNN network, as in-built feature engineering capability is a main highlight of

(a) WA

(b) NSW

(c) Mixed

Fig. 9. Scree plots of the PCA applied to the dataset corresponding to the (a) WA, (b) NSW, and (c) mixed observations.

standing trees were tested in WA, of which ten were flawed and nine were healthy. The health state of the trees was determined after cutting and performing a visual inspection. However, the trees were tested before cutting, and there were 822 ultrasonic signals collected from the sampled trees at breast height. The optimal MLAs, i.e., Fine Gaussian SVM and the 1D-CNN models (with all and selected features) trained on the billets harvested from WA, NSW, and their mixture, were employed to estimate the health condition of the trees. The final accuracy results are reported in Table 14. It was generally expected to achieve poor accuracy when applying the trained models on NSW species for estimating the label of the trees in WA. The results of the table indicate that this is the case.

Moreover, it can be seen from the table that the Fine Gaussian SVM model trained on the WA billets provides the highest accuracy of 87.4%, followed by the 1D-CNN with all the features trained on WA billets at 85.5%. However, the accuracy obtained from the 1D-CNN with selected features trained on the mixture of billets was 84.8%–more than the Fine Gaussian SVM at 78.4% and the 1D-CNN model with all the features at 78%. Interestingly, the 1D-CNN model with selected features and all features trained on the NSW specimens performs relatively better than the Fine Gaussian model with an accuracy of 64.4 and 65.8 percent, respectively, where the poorest results were obtained from the Fine Gaussian model trained on NSW billets with 58.9% accuracy.

The results of Table 14 again confirm our previous observation. As such, one can see that the performance of the trained model of mixed samples has significantly (6.8%) improved by using the selected features. This is while this accuracy slightly worsened in models trained on WA and NSW samples by 1 and 1.4 percent, respectively.

Table 13

The 5-fold cross-validation accuracy results obtained for the training and test sets using the trained 1D-CNN models with all features.

Accuracy (%)	WA	NSW	Mixed
Training	98	99.9	98.8
Testing	93	97.6	94

Table 14

The testing accuracy (%) of the trained CNN models on test data collected from standing trees in WA.

Model	WA	Mixed	NSW
CNN (selected features)	84.5	84.8	64.4
CNN (all features)	85.5	78	65.8
Fine Gaussian SVM	87.4	78.4	58.9

6. Future work

In Section 5, the developed models were further tested on some standing trees. Based on the results, it is more generalizable to predict the label of unseen data in WA using 1D-CNN trained on mixed samples with selected features as opposed to the model, which is trained using all features. However, the presented accuracy results were not intended for decision-making about accepting or rejecting the null hypothesis that a tested tree is healthy. This is mainly due to the fact that it is not clear how to decide the integrity of a tree whose, for instance, more than 50% test outcomes are negative, but still, a few are positive. Some internal defects in the wooden sections may not be deemed significant
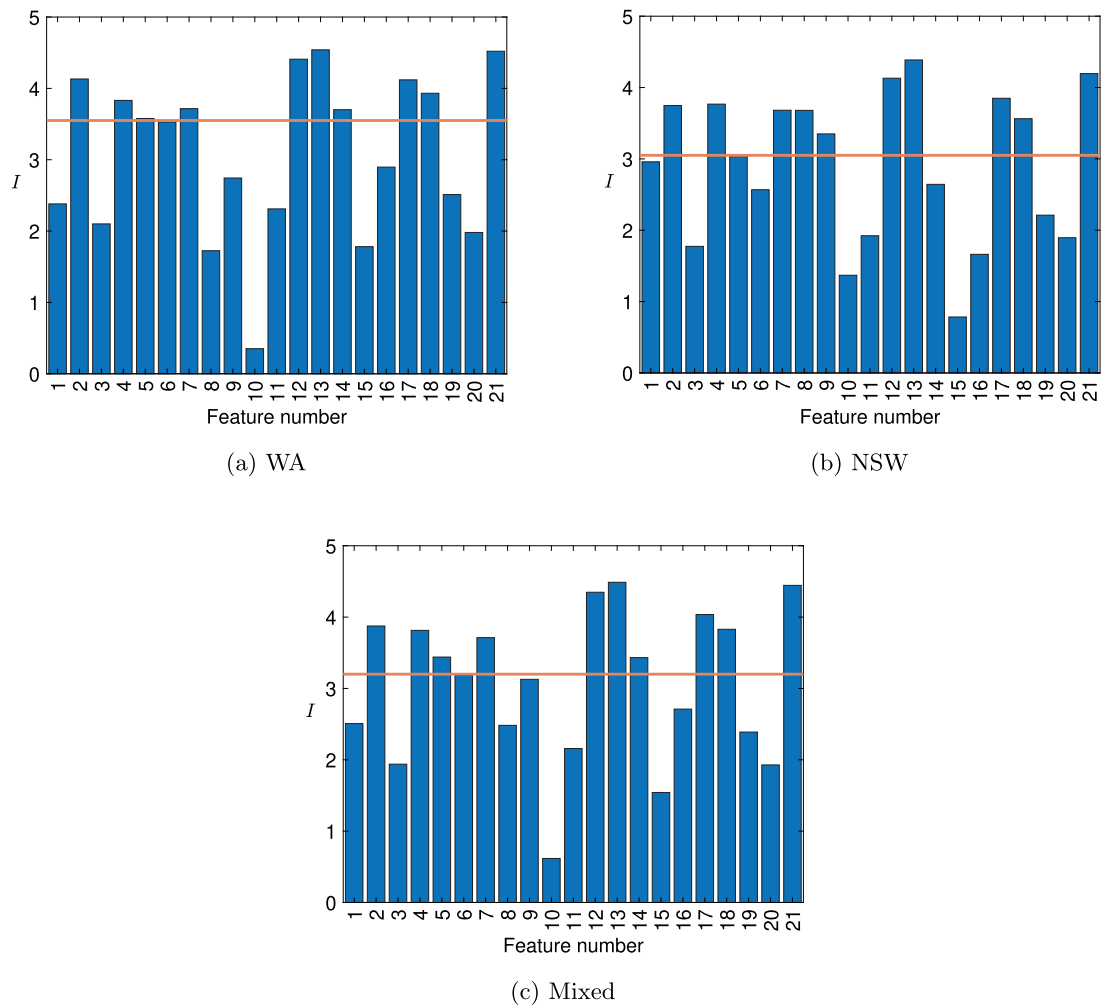
(a) WA

(b) NSW

(c) Mixed

Fig. 10. Contribution percentage of each feature to the first principal dimension for (a) WA, (b) NSW, (c) mixed observations.
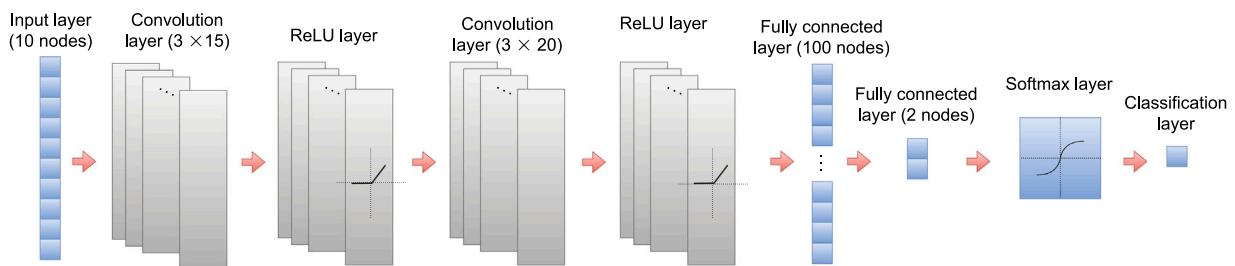

Fig. 11. The architecture of the constructed 1D-CNN.

defects and may not thus exclude the tree from being used for industrial purposes. For such defects, it is evident that the test results obtained from testing from certain angles may be positive. This is schematically demonstrated in Fig. 12. Therefore, further work needs to be done on the decision-making part of the proposed strategy to make assigning a label to a tested tree more rational for practical applications. This can indeed be a potential subject of future work.

In this study, different models were trained for test data collected in the lab and field. One possible future work could be employing the concept of transfer learning, where models trained on lab specimens will be generalized for use in the field. Moreover, the extracted features can be expanded by deriving statistical features from the instantaneous amplitude of IMFs obtained from ultrasonic test results.

7. Conclusions

The problem of wood quality assessment of standing trees has been targeted by solving the classification problem of trees using contact–ultrasonic testing and machine learning algorithms. To this end, the contact–ultrasonic test results were first decomposed into their constituent components using the VMD algorithm to derive informative features. The importance of each feature was identified through a new equation based on the loading of each feature obtained from the PCA analysis of the feature matrix. Several test results were obtained from lab specimens, and samples from sites of the two states in Australia, i.e., WA and NSW, were studied. The results of the lab trial were
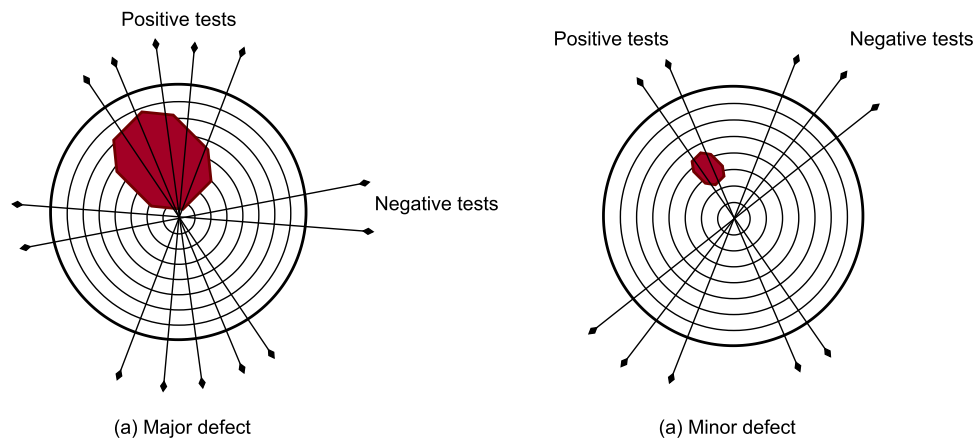
Fig. 12. Testing a cross-section of a tree with (a) major defect and (b) minor defect.

matched with those obtained in the field. As such, the Fine Gaussian SVM was shown to be the most effective MLA for solving the classification problem in both cases. Moreover, it was shown that in both cases, features corresponding to σ_{IF} of IMF_3, $Q2_{IF}$ of IMF_3, $Q1_{IF}$ of IMF_3, and $Q1_{IF}$ of IMF_2 were most valuable features to be used for classification. This indicates features extracted from high-frequency IMFs are of significant importance, further supporting the idea of signal decomposition.

A 1D-CNN model was constructed to solve the classification problem of billets obtained from trees harvested in the fields. The results indicate the Fine Gaussian algorithm and 1D-CNN can effectively solve the problem of wood classification in the fields. In the worst case, using the selected features led to achieving 92.2% accuracy for the mixture of billets obtained from WA and NSW sites. The 1D-CNN model was also trained using all the extracted features and compared with the model results when using selected features. The results show that training the model with selected features could improve model performance in most cases. Also, it was noted that the performance of the CNN model slightly declined in some other cases. Overall, the proposed feature selection algorithm produces a robust classification of wood specimens based on their health condition. The trained models were then employed to predict the health status of standing trees at WA sites. According to the results, it is apparent that the 1D-CNN model is more generalizable in all cases. However, this hypothesis needs to be further tested by applying the models to larger data sets.

In summary, the results of this study pave the way for solving the problem of determining the health status of wood. This paper's results also confirm the VMD algorithm's effectiveness in obtaining time–frequency features from ultrasonic signals. Further work is needed on the decision-making portion of the problem, in which test results from different angles on a cross-section of a tree (mainly breast height) are used to discern whether the timber is helpful for industrial applications.

CRediT authorship contribution statement

Mohsen Mousavi: Conceptualization, Visualization, Methodology, Software, Validation, Formal analysis, Investigation, Resources, Data curation, Writing – original draft. **Mohammad Sadegh Taskhiri:** Conceptualization, Investigation, Resources, Data curation. **Amir H. Gandomi:** Conceptualization, Visualization, Writing – review & editing, Supervision, Project administration, Funding acquisition.

Declaration of competing interest

The authors declare that they have no known competing financial interests or personal relationships that could have appeared to influence the work reported in this paper.

Data availability

The authors do not have permission to share data.

References

Abid, A., Khan, M.T., Iqbal, J., 2021. A review on fault detection and diagnosis techniques: basics and beyond. Artif. Intell. Rev. 54 (5), 3639–3664.

Blomme, E., Bulcaen, D., Declercq, F., 2002. Air-coupled ultrasonic NDE: experiments in the frequency range 750 kHz–2 MHz. NDT E Int. 35 (7), 417–426.

Dackermann, U., Skinner, B., Li, J., 2014. Guided wave–based condition assessment of in situ timber utility poles using machine learning algorithms. Struct. Health Monit. 13 (4), 374–388.

Dragomiretskiy, K., Zosso, D., 2014. Variational mode decomposition. IEEE Trans. Signal Process. 62 (3), 531–544.

El Najjar, J., Mustapha, S., 2021. Condition assessment of timber utility poles using ultrasonic guided waves. Constr. Build. Mater. 272, 121902.

EN 408:2010+A1:2012, 2010. EN 408:2010+A1:2012 – Timber Structures, Structural Timber and Glued Laminated Timber, Determination of Some Physical and Mechanical Properties. Standard, European Standards.

Fang, Y., Lin, L., Feng, H., Lu, Z., Emms, G.W., 2017. Review of the use of air-coupled ultrasonic technologies for nondestructive testing of wood and wood products. Comput. Electron. Agric. 137, 79–87.

Fathi, H., Kazemirad, S., Nasir, V., 2021. Lamb wave propagation method for non-destructive characterization of the elastic properties of wood. Appl. Acoust. 171, 107565.

Fathi, H., Nasir, V., Kazemirad, S., 2020. Prediction of the mechanical properties of wood using guided wave propagation and machine learning. Constr. Build. Mater. 262, 120848.

Gabor, D., 1946. Theory of communication. Part 1: The analysis of information. J. Inst. Electr. Eng.-Part III: Radio Commun. Eng. 93 (26), 429–441.

Gao, S., Wang, N., Wang, L., Han, J., 2014. Application of an ultrasonic wave propagation field in the quantitative identification of cavity defect of log disc. Comput. Electron. Agric. 108, 123–129.

Goh, C.L., Rahim, R.A., Rahiman, M.H.F., Talib, M.T.M., Tee, Z.C., 2018. Sensing wood decay in standing trees: A review. Sensors Actuators A 269, 276–282.

Handbook, C., Wood, 1999. Wood as an Engineering Material. Forest Products Laboratory. Gen. Tech. Rep. FPL–GTR–113, USDA Product Society, Madison, Wisconsin, USA.

Hassani, S., Mousavi, M., Gandomi, A.H., 2022a. Damage detection of composite laminate structures using VMD of FRF contaminated by high percentage of noise. Compos. Struct. 286, 115243.

Hassani, S., Mousavi, M., Sharif-Khodaei, Z., 2022b. Smart bridge monitoring. In: The Rise of Smart Cities. Elsevier, pp. 343–372.

Karaiskos, G., Deraemaeker, A., Aggelis, D., Van Hemelrijck, D., 2015. Monitoring of concrete structures using the ultrasonic pulse velocity method. Smart Mater. Struct. 24 (11), 113001.

Khan, A., Sohail, A., Zahoora, U., Qureshi, A.S., 2020. A survey of the recent architectures of deep convolutional neural networks. Artif. Intell. Rev. 53 (8), 5455–5516.

Krajnc, L., Kadunc, A., Straže, A., 2019. The use of ultrasound velocity and damping for the detection of internal structural defects in standing trees of European beech and Norway spruce. Holzforschung 73 (9), 807–816.

Lei, T., Yang, S.-Y., Tobin, B., O'Reilly, C., Sun, D.-W., 2022. A measurement framework using THz time-domain sensing for wood quality assessment across tree ring samples. Comput. Electron. Agric. 202, 107437.

Li, W., Van den Bulcke, J., Mannes, D., Lehmann, E., De Windt, I., Dierick, M., Van Acker, J., 2014. Impact of internal structure on water-resistance of plywood studied using neutron radiography and X-ray tomography. Constr. Build. Mater. 73, 171–179.

Lin, C.-J., Kao, Y.-C., Lin, T.-T., Tsai, M.-J., Wang, S.-Y., Lin, L.-D., Wang, Y.-N., Chan, M.-H., 2008. Application of an ultrasonic tomographic technique for detecting defects in standing trees. Int. Biodeterioration Biodegrad. 62 (4), 434–441.

Liu, J., Zhou, J., Qi, S., Cui, Z., Wang, K., 2013. Influence of texture anisotropy on acoustoelastic birefringence in stressed wood. J. Acoust. Soc. Am. 134 (5), 4227.

López, G., Basterra, L.A., Acuña, L., 2013. Estimation of wood density using infrared thermography. Constr. Build. Mater. 42, 29–32.

Mackenzie-Helnwein, P., Eberhardsteiner, J., Mang, H.A., 2003. A multi-surface plasticity model for clear wood and its application to the finite element analysis of structural details. Comput. Mech. 31 (1–2), 204–218.

Mori, M., Hasegawa, M., Yoo, J.-C., Kang, S.-G., Matsumura, J., 2016. Nondestructive evaluation of bending strength of wood with artificial holes by employing air-coupled ultrasonics. Constr. Build. Mater. 110, 24–31.

Mousavi, M., Gandomi, A.H., 2021. Wood hole-damage detection and classification via contact ultrasonic testing. Constr. Build. Mater. 307, 124999.

Mousavi, M., Taskhiri, M.S., Holloway, D., Olivier, J., Turner, P., 2020. Feature extraction of wood-hole defects using empirical mode decomposition of ultrasonic signals. NDT E Int. 102282.

Muskhelishvili, I., Radok, J.R.M., 2008. Singular Integral Equations: Boundary Problems of Function Theory and their Application to Mathematical Physics. Courier Corporation.

Nasir, V., Fathi, H., Kazemirad, S., 2021. Combined machine learning–wave propagation approach for monitoring timber mechanical properties under UV aging. Struct. Health Monit. 20 (4), 2035–2053.

Palander, T., Eronen, J., Kärhä, K., Ovaskainen, H., 2018. Development of a wood damage monitoring system for mechanized harvesting. Ann. Forest Res. 61 (2), 243–258.

Pang, S.-J., Shim, K.-B., Kim, K.-H., 2021. Effects of knot area ratio on the bending properties of cross-laminated timber made from Korean pine. Wood Sci. Technol. 55 (2), 489–503.

Pedram, S.K., Mudge, P., Gan, T.-H., 2018. Enhancement of ultrasonic guided wave signals using a split-spectrum processing method. Appl. Sci. 8 (10), 1815.

Ramage, M.H., Burridge, H., Busse-Wicher, M., Fereday, G., Reynolds, T., Shah, D.U., Wu, G., Yu, L., Fleming, P., Densley-Tingley, D., et al., 2017. The wood from the trees: The use of timber in construction. Renew. Sustain. Energy Rev. 68, 333–359.

Reinprecht, L., Pánek, M., 2012. Ultrasonic technique for evaluation of bio-defects in wood: Part 1–Influence of the position, extent and degree of internal artificial rots. Int. Wood Prod. J. 3 (2), 107–115.

Senalik, A.C., Schueneman, G., Ross, R.J., 2014. Ultrasonic-Based Nondestructive Evaluation Methods for Wood: a Primer and Historical Review. General Technical Report, FPL-GTR-235, USDA Forest Service, Forest Products Laboratory, pp. 1–36, 2014; 36 p. 235.

Tallavo, F., Cascante, G., Pandey, M.D., 2012. A novel methodology for condition assessment of wood poles using ultrasonic testing. NDT E Int. 52, 149–156.

Taskhiri, M.S., Hafezi, M.H., Harle, R., Williams, D., Kundu, T., Turner, P., 2020. Ultrasonic and thermal testing to non-destructively identify internal defects in plantation eucalypts. Comput. Electron. Agric. 173, 105396.

Yaitskova, N., van de Kuilen, J.W., 2014. Time-of-flight modeling of transversal ultrasonic scan of wood. J. Acoust. Soc. Am. 135 (6), 3409–3415.

Yang, H., Yu, L., 2017. Feature extraction of wood-hole defects using wavelet-based ultrasonic testing. J. Forest. Res. 28 (2), 395–402.

Zosso, D., 2020. Variational mode decomposition, MATLAB central file exchange. Retrieved August 27, 2020. URL: https://www.mathworks.com/matlabcentral/fileexchange/44765-variational-mode-decomposition.